

All at once: transient pulsations, spin down and a glitch from the Pulsating Ultraluminous X-ray Source M82 X-2

MATTEO BACHETTI,^{1,2,*} THOMAS J. MACCARONE,³ MURRAY BRIGHTMAN,² MCKINLEY C. BRUMBACK,⁴ FELIX FÜRST,⁵
FIONA A. HARRISON,² MARIANNE HEIDA,² GIAN LUCA ISRAEL,⁶ MATTHEW J. MIDDLETON,⁷ JOHN A. TOMSICK,⁸
NATALIE A. WEBB,⁹ AND DOMINIC J. WALTON¹⁰

¹*INAF-Osservatorio Astronomico di Cagliari, via della Scienza 5, I-09047 Selargius, Italy*

²*Space Radiation Laboratory, Caltech, 1200 E California Blvd, Pasadena, CA 91125*

³*Department of Physics and Astronomy, Texas Tech University, Lubbock, TX, USA*

⁴*Department of Physics & Astronomy, Dartmouth College, 6127 Wilder Laboratory, Hanover, NH 03755, USA*

⁵*European Space Astronomy Centre (ESA/ESAC), Operations Department, Villanueva de la Canada Madrid, Spain*

⁶*Osservatorio Astronomico di Roma, INAF, via Frascati 33, I-00078 Monte Porzio Catone, Italy*

⁷*Department of Physics and Astronomy, University of Southampton, Highfield, Southampton SO17 1BJ, UK*

⁸*Space Sciences Laboratory, University of California, Berkeley, 7 Gauss Way, Berkeley, CA 94720, USA*

⁹*IRAP, Université de Toulouse, CNRS, UPS, CNES, 9 Avenue du Colonel Roche, BP 44346, 31028 Toulouse Cedex 4, France*

¹⁰*Institute of Astronomy, University of Cambridge, Madingley Road, Cambridge CB3 0HA, UK*

ABSTRACT

M82 X-2 is the first pulsating ultraluminous X-ray source (PULX) to be identified. Since the discovery in 2014, *NuSTAR* has observed the M82 field 15 times throughout 2015 and 2016. In this paper, we report the results of pulsation searches in all these datasets, and find only one new detection. This new detection allows us to refine the orbital period of the source and measure an average spin down rate between 2014 and 2016 of $-5 \cdot 10^{-11}$ Hz/s, which is in contrast to the strong spin up seen during the 2014 observations and represent the first detection of spin down in a PULX system. Thanks to the improved orbital solution allowed by this new detection, we are also able to detect pulsations in additional segments of the original 2014 dataset. We find a glitch superimposed on the very strong and variable spin-up already reported, the first positive glitch identified in a PULX system. We discuss the new findings in the context of current leading models for PULXs.

Keywords: stars: neutron — pulsars: individual (M82 X-2) — X-rays: binaries — ULX

1. INTRODUCTION

Ultraluminous X-ray sources are off-nuclear point sources with X-ray luminosities exceeding the Eddington limit for a stellar-remnant black hole. In 2014, Bachetti et al. (2014) (hereafter B14) reported pulsations from the known ULX M82 X-2, showing that at least some of them are neutron stars. With additional observations and timing analysis, more of these objects are being found to pulsate (e.g. NGC 5907 X-1: Israel et al. 2017a; NGC 7793 P13: Israel et al. 2017b; Fürst et al. 2016; NGC 300 X-1: Carpano et al. 2018). The spectral and variability properties of the PULXs are similar to the bulk of the ULX population. Looking in detail, they tend to have slightly harder spectra and

a higher level of long term-variability than average¹. This fact, together with the intrinsic difficulties in finding pulsations in these distant sources; they are often in binaries and show strong spin variations on short time scales, means it is plausible that most of the ULX population is powered by neutron stars².

The Pulsating ULXs found so far have in common periods around 1 s (with the notable exception of NGC 300 X-1), and strong spin-ups during observations and between observations spaced apart months to years.

After the discovery of pulsations from M82 X-2, we obtained a long *NuSTAR* observation of the pulsar with the aim of detecting pulsations and, through the mea-

¹ For a detailed view see Pintore et al. 2017; Walton et al. 2018; Koliopanos et al. 2017

² (for deeper investigations of ULX populations, see Middleton & King 2017; Wiktorowicz et al. 2018)

surement of a possible orbital shrinking, constrain the total mass exchange in the system. The observation was performed on UT 2016-04-15 – 2016-04-19 (MJDs 57493.29 – 57497.34). *NuSTAR* does not resolve M82 X-2 from another ULX, M82 X-1, only 5'' away. This source is known to reach luminosities an order of magnitude higher than M82 X-2, and only *Chandra* is able to resolve the two ULXs. Therefore, we undertook another program to monitor M82 monthly with *Chandra* with 25 ks per pointing with simultaneous *NuSTAR* 40 ks pointings. This *Chandra-NuSTAR* program was designed to study the spectral evolution of the two sources, as well as to characterize the overall binary population in the galaxy (see Brightman et al. 2019, Brightman et al. in prep.).

In this Paper, we present the timing analysis the new data from the monitoring program, and show that the pulsations are only detected in one new observation, despite the fact that in some cases *Chandra* infers flux levels of M82 X-1 and M82 X-2 that should allow a detection. Revisiting the work by B14, we show that the pulsed fraction evolves independently from the flux from the nearby M82 X-1, showing that this behavior is intrinsic to M82 X-2. Thanks to the new detection, we are able to measure the orbital period of the system with greater precision, recover pulsations in one more old observation and detect a pulsar glitch.

In Section 2 we describe the data reduction procedure. In Section 3 we detail the pulsation searches performed and report on the new pulsations, the orbit and spin measurements. We discuss the results in Section 4 and 5.

2. DATA REDUCTION

The observations considered in this work are detailed in Table 2. For *NuSTAR* used data processed with *nupipeline* shipped with HEASOFT v.6.25, with standard options. We barycentered the data in two independent ways: on one side, we used the FTOOL *barycorr* with the standard CALDB clock file; on the other, we tested a new temperature-driven model of the clock offsets, under development (Bachetti, Markwardt et al. in prep), and used PINT³ for the satellite orbit calculations. The pulse period of M82 X-2 is three orders of magnitude longer than the observed difference between the two barycentering methods. For the orbit file, we used the attitude-orbit file produced by *nupipeline*⁴. The pipeline ran using default values left some intervals

of increased background activity (probably due to the South-Atlantic Anomaly), producing spikes in the light curve. We verified that that the spikes corresponded to increased activity on the entire field of view and not just from a single source in the field of view, and remove the relevant intervals by modifying the good time intervals (GTI). Following B14, we selected photons from a region of 70'' around M82 X-2. This region contains a large number of X-ray sources (e.g. B14), with the total flux typically dominated by the combination of M82 X-1 ($L_{x,peak} \sim 1 \cdot 10^{41}$ erg/s) and M82 X-2 ($L_{x,peak} \sim 2 \cdot 10^{40}$ erg/s). Given their ~5'' separation, it is not possible to disentangle the contribution from these two sources to the *NuSTAR* data, so they must be considered together.

We did not redo the *Chandra* data reduction, and we used the data from Brightman et al. (2019) and Brightman et al. *sub.*

3. SEARCH FOR PULSATIONS AND RESULTS

We used a number of methods to detect new pulsations from M82 X-2, ranging from a focused search around the known frequency values and orbital parameters to a quasi-blind search (allowing for very large variations of the pulse frequency).

Data analysis was done through a set of custom python scripts based on HENDRICS⁵ (Bachetti 2018), Stingray⁶ (Huppenkothen et al. 2019; Huppenkothen et al. 2016) PINT (Luo et al. 2019), and PRESTO (Ransom 2011, 2001).

In the 2-Ms long campaign performed in 2014, where the pulsar was first detected, pulsations did not have a constant r.m.s. A large variation of pulsed fraction was reported by B14 and is also shown in Fig. 7. Orbital motion represented an additional difficulty. In fact, in 2014 the pulsar was initially detected only after the pulsed fraction had increased well above the detection level, because orbital motion smears out the observed pulsed frequency and the fainter signal was dominated by the white noise. Only after the first orbital parameter calculation, obtained in the observations at high pulsed fraction, the pulse was found in some of the previous observations.

Therefore, any search for pulsations in new observations had to account for at least two complications: faint pulsations, strong spin up and orbital motion. We used a two-tiered approach to this search: a deep search for

³ www.github.com/nanograv/PINT

⁴ During the study of the temperature-driven model for the spacecraft clock, we realized that the orbit file distributed in the

auxiliary data of *NuSTAR* observations, and recommended for use with *barycorr*, did not account properly for leap seconds.

⁵ www.github.com/StingraySoftware/HENDRICS

⁶ www.github.com/StingraySoftware/stingray

Table 2. Pulsation search results from all available observations of M82 X-2.

ObsID	MJD	Date	Length ^a	Exposure ^a	Count rate ^b	Meas. p.f. ^c	Est. Flux ratio ^d	Corr. p.f. ^e
			(ks)	(ks)	(s ⁻¹)	$\Delta F_{X2}/F_{\text{tot}}$	$F_{X2}/F_{X1}(\%)$	$\Delta F_{X2}/F_{X2}$
80002092002	56681	2014-01-23	123	66	0.9	<5%	—	—
80002092004 ^f	56683	2014-01-25	171	90	1.0	4%	—	—
80002092006	56686	2014-01-28	579	310	0.9	5%	—	—
80002092007	56692	2014-02-04	562	306	0.9	7%	132%*	12%
80002092008	56699	2014-02-10	62	34	1.0	7%	—	—
80002092009	56700	2014-02-11	213	115	0.9	9%	—	—
80002092011	56720	2014-03-03	201	111	0.6	3%	—	—
50002019002	57038	2015-01-15	56	31	0.7	<6%	40%	<21%
50002019004	57042	2015-01-19	283	161	0.7	<4%	33%*	<17%
90101005002	57194	2015-06-20	56	37	2.3	<3%	32%	<14%
80202020002	57414	2016-01-26	66	36	1.5	<4%	0%*	N.A.
80202020004	57442	2016-02-23	61	32	1.3	<5%	52%	<14%
80202020006	57483	2016-04-05	54	31	0.8	<6%	44%	<20%
30101045002	57493	2016-04-15	350	189	1.0	<3%	—	—
80202020008	57503	2016-04-24	67	40	1.1	<5%	79%	<11%
30202022002	57543	2016-06-03	60	39	1.0	<5%	0%*	N.A.
30202022004	57571	2016-07-01	68	47	1.7	<4%	33%	<14%
30202022008	57599	2016-07-29	67	43	1.6	<4%	4%*	N.A.
30202022010	57619	2016-08-19	69	44	1.2	<4%	16%*	<31%
90201037002	57641	2016-09-10	94	80	1.2	3%	—	—
90202038002	57669	2016-10-07	71	45	0.9	<5%	5%*	N.A.
90202038004	57723	2016-11-30	68	43	0.8	<5%	0%*	N.A.
Total detected			1000 (58%)					
Total undetected			730 (42%)					
M82 X-2 flux too low			207					

^aThe Length of the observation is the UT stop time minus the UT start time. The Exposure is the actual on-source time not including occultation from the Earth and other “bad” intervals.

^bCount rates using FPMA + FPMB

^cThe pulsed fraction is referred to the total X-ray flux of M82, since M82 X-1 and X-2 are not separable in *NuSTAR*

^dThe flux ratio between M82 X-2 and M82 X-1 is estimated from *Chandra* data, either from the detailed and pileup-corrected spectral modeling of Brightman et al. in prep. when available, or from Brightman et al. (2019) otherwise (starred). Dashes indicate that a *Chandra* dataset was not available.

^eA corrected estimate of the pulsed fraction, when a flux ratio is available. *Not Allowed* (N.A.) indicates that the pulsed flux should be higher than the flux measured by *Chandra*

^fDetected only after MJD 56683.5

NOTE—Intervals where M82 X-2 is weaker than 10% M82 X-1 are not counted in the statistics of non-detections.

pulsations around the expected spin period values and orbital parameters, and a more general search using multiple spin derivatives on 40-ks segments of data.

We report the details in the following subsections.

3.1. Deep pulsation searches - first pass

The first attempt consisted of a deep search of pulsations using the Z_2^2 statistics (Buccheri et al. 1983). The Z_2^2 statistics was calculated from the functions in `stingray` and `HENDRICS`⁷.

We varied the frequency between the observed frequency in 2014 and the maximum frequency expected from a constant source spin-up of $5 \cdot 10^{-10}$ Hz/s (more than double the maximum spin up observed in 2014). The choice of the frequency interval was driven primarily by computing time and using an acceptable number of trial values. The frequency step was 8 times finer than the standard (e.g. FFT) $\delta\nu = 1/T$, with T the observing time. This was to avoid the effects of spectral leakage on weak pulsations (e.g. see discussion on “interbinning” by Ransom et al. 2002). Not finding new detections above the standard $3 - \sigma$ detection level accounting for the number of trials, we shifted the orbital phase by trial values spaced by 500s in order to account for a possibly imperfect orbital solution. Again (and taking into account the increased number of trials), we did not find new significant pulsations with this strategy.

3.2. Accelerated search

We used the PRESTO suite of pulsar search programs (Ransom 2001; Ransom et al. 2002) to run two different techniques of pulsation search, one Fourier-based (with the tool `accelsearch`) and one epoch folding-based (with the tool `prepfold`).

Following the strategy adopted in 2014, we split the light curves in segments of 30 ks, with sliding windows overlapping by a factor ~ 0.5 . This is motivated by the following: a longer light curve in principle allows to accumulate more signal in the periodograms, but orbital motion smears the signal of an accelerated search if the length is more than a certain fraction of the orbital period (the usual rule-of-thumb is $1/7$ of P_{orb}). This was clearly seen in the the 2014 campaign, where the maximum detectability with the accelerated methods in `prepfold` was indeed obtained with segments of 30 ks, or about $1/7P_{\text{orb}}$.

⁷ Rather than calculating the Z_n^2 statistics on the single events, this software pre-folds the data and then calculates the statistics using the phases of the profile with a weight given by the number of counts in each profile bin (Huppenkothen et al. 2019)

We binned the light curves to 1 ms, and produced binary floating point datasets in a format understandable by PRESTO using the `HENbinary` script in `HENDRICS`.

We first used the `accelsearch` tool, that performs an accelerated search of pulsations based on the Fast Fourier Transform and matched filters. We used the lowest detection limit (`-sigma=1` on the command line), and specified that data were obtained by photons (`-photon`). A number of “candidates” (possible signals above the threshold power value) were produced by this search and followed-up with `prepfold` to evaluate the significance using epoch folding. All candidate periods from this search were very different from the reasonable interval of pulsations from M82 X-2. We could also safely dismiss the possibility that these candidates were from other pulsars in the field of view, as the candidate pulsations always had very low significance and were not consistent between segments of data, as one would expect instead from pulsar candidates. Some of these candidates are suspiciously close to beats of fundamental frequencies of the NuSTAR detector (e.g. the CP mode oscillation at ~ 890 Hz) or to the orbital data gaps.

We next tried to use the tool `prepfold` to run an epoch folding-based search (i.e., suggesting candidate periods instead of letting `accelsearch` do so). `prepfold` automatically searches the $p - \dot{p}$ plane, including all reasonable \dot{p} values expected from the source if the interval length is 30 ks. Even if the maximum \dot{p}_{spin} in 2014 was high, many accreting pulsars have an averaged \dot{p}_{spin} much smaller than the instantaneous value found in single observations, due to the alternation of spin-up and spin-down events that the accretion torque produces when accretion rate increases and decreases. Therefore, we suggested a starting value of the period around the mean value in 2014, and then used a number of starting values further and further from the mean value in both directions, randomly distributed in an interval larger than ten times the period variation expected if the maximum \dot{p}_{spin} in 2014 was constant until our new observations (which would result in spin periods of 1.31-1.372 s). The random distribution allowed a certain amount of duplication (to test if a good candidate was consistently found with similar starting periods) and to avoid grid-related issues. Still, no significant new pulsations were found. To evaluate a rough significance, we used the probability to find a given number of σ from a search over 1000 realizations of white noise, using the same GTIs as the original observations.

3.3. The “Jerk” search and a new detection in 2016

Finally, we took advantage of the recently developed “Jerk” search technique in `accelsearch` (Andersen & Ransom 2018). This time, since this technique uses both the first and the second frequency derivatives, we used longer chunks of data, around 80 ks (when the observation was long enough). Thanks to the “Jerk” search, we found one new candidate pulsation in ObsID 90201037002.

New orbital solution—We refined the candidate from the “Jerk” search with `prepfold`, and local values of the period and two period derivatives were measured with precision. They were consistent with those expected from a ~ 1.37 s pulsation Doppler shifted by orbital motion with $P_{orb} \sim 2.52$ d and $a \sin i/c \sim 22$ lt-sec, the orbital parameters known from B14. We refined the spin solution using the full observation (instead of a 80-ks segment) using `HENphaseogram`⁸. These local spin derivatives give effects two orders of magnitude above the reasonable interval for the spin up of the source, which is $|\dot{\nu}| \lesssim 2 \cdot 10^{-10}$ Hz/s. Despite the observation covering less than 1/3 of an orbit, the measured spin derivatives were sufficient to put a constraint on the orbital phase (Fig. 1). We can expect intrinsic (torque-driven) spin-up or spin-down whose magnitude is up to some 10^{-10} s/s. The spin-up parameters and the orbital parameters are degenerate, and we include these considerations when calculating the improved error bar on the orbital period P_{orb} .

Nonetheless, the 2.5-year lever arm between this new measurement and the original 2014 dataset allows to reduce the error bar on P_{orb} to be reduced significantly. We find that the value of T_0 inferred from this observation is close, even if outside the range allowed by the quoted error bar on P_{orb} from the solution by B14. We will discuss the possible implications in Section 4.2.

Later, we tested the possibility that an integer number of additional orbital periods could fit into the time range between ObsIDs 80002092011 and 90201037002. An error on the period of ~ 0.0001 d, as implied by an additional or missing full orbit in this time range, would produce a very obvious distortion of the 2014 solution, and this possibility can be safely neglected (See Fig. 2, bottom panel).

Spin down—The most intriguing and unquestionable consequence of this new detection is that, contrary to all other pulsating ultraluminous X-ray sources found until now, between 2014 and 2016 the source showed an average spin *down* (Fig. 4) of $\dot{\nu} \sim -5.8 \cdot 10^{-11}$ Hz/s.

The spin down observed between 2014 and 2016 is likely to be driven by the negative torque of an accretion disk. The alternating behavior between spin up and spin down suggests that the source is close to spin equilibrium, validating the assumption in the torque and magnetic field estimates by B14. An additional component could be dipole radiation from a strong magnetic field. We discuss the implications of this finding in Section 4.2.

3.4. Deep pulsation searches with new orbital solution, and upper limits.

Based on the improved orbital solution described in Section 3.3.0.0, we ran a deeper search using the Z_1^2 (Rayleigh test) and Z_2^2 statistics (Buccheri et al. 1983). Given the unexpected new spun-down frequency, this new search included a much larger interval of frequencies but a better constraint on the orbital phase. This time, we also ran simulations to evaluate the pulsed fraction upper limit in non-detections. To do so, for each dataset, we maintained the GTIs and the total number of photons in each interval and randomized the time of the events inside the each GTI. There is no significant broad-band noise at the frequency of the pulsar. Again, we used the statistical functions in `stingray` and `HENDRICS`. As discussed above, this software allows to calculate the statistics from the folded profiles instead of the single events as in the original Rayleigh test and Buccheri et al. (1983). To speed up further the calculation (in particular when calculating the larger number of realizations required by the upper limit calculations), we executed the total folding by folding M equal-length sub-intervals of the observations, and aligning the folded sub-profiles differently for slightly different values of the frequency (similarly to the Fast Folding Algorithm, Taylor & Weisberg 1982, and the technique used in `prepfold`). A bonus of this technique is that it is easy to shift the sub-intervals by integer values according to linear, quadratic, and higher-order laws and measure rapid changes of different spin frequencies. The main rules-of-thumb to avoid dispersion of the signal in multiple bins are 1) that the number of bins in the profile N is large enough that the pulse shape features are distinct in different bins and 2) that the number of profiles that are being shifted is at least twice the maximum shift of the sub-profiles. We verified that calculating these statistical tests this way does not depart significantly from the expected statistics (More details in the Appendix and 7). Using this method, we do not find significant detections in new observations. As expected from the decrease of trial values and the better description of the data given by the orbital solution instead of a few spin derivatives, the detection in 90201037002 turns out to

⁸ The signal-to-noise in single intervals was not adequate to make more sophisticated timing using, e.g. `PINT` or `tempo2`

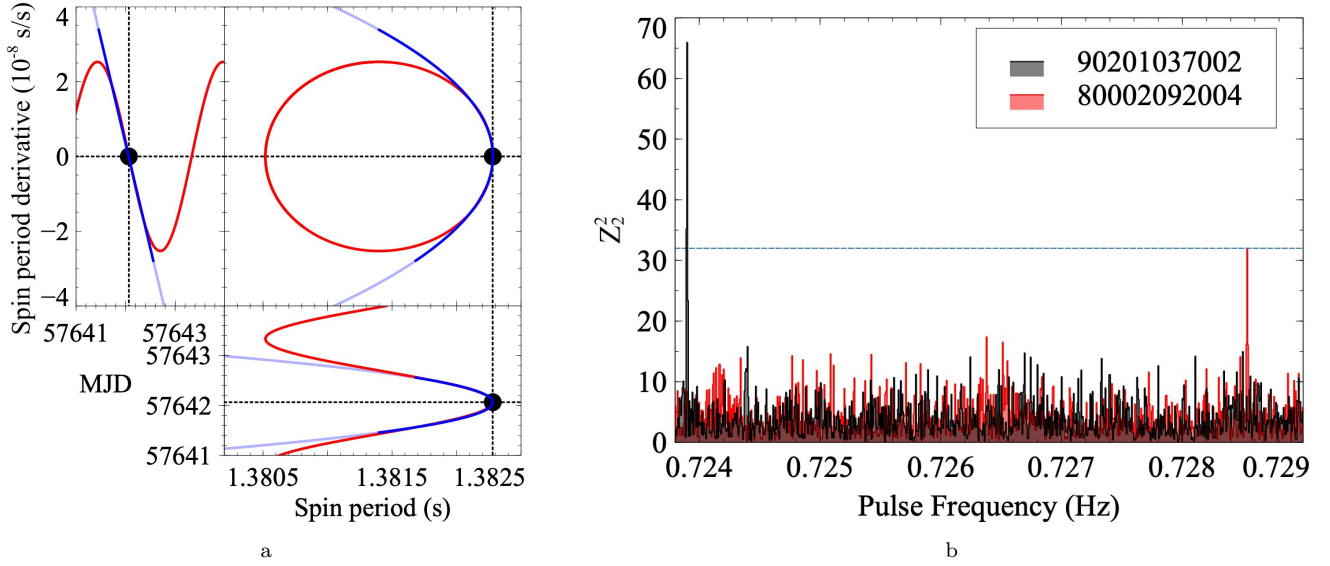


Figure 1. (a) The orbital phase can be measured from the spin solution if a measurement of at least two spin frequency derivatives ($\dot{\nu}$, $\ddot{\nu}$) is available. Here we compare the best spin solution calculated by PRESTO (cyan, and blue in the time range covered by the data) and the expected ν and $\dot{\nu}$ change due to the orbital Doppler effect (red). At this phase of the orbit, the constraint on the ascending node passage is very accurate. (b) The new detections in ObsID 90201037002 and 80002092004, using the all-data orbital solution in Table 4. The horizontal line indicates the 3- σ detection level for the given number of trial frequencies.

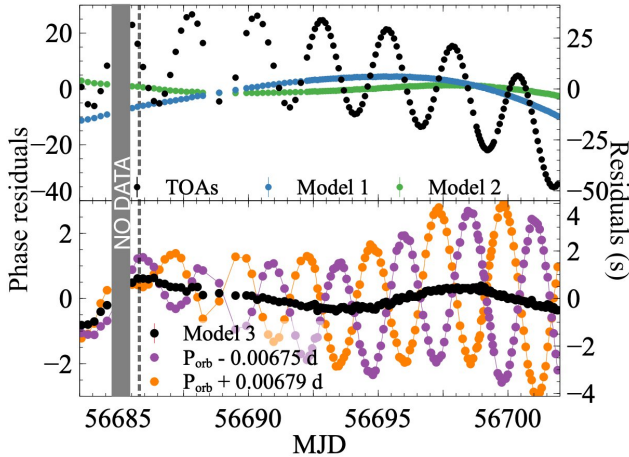


Figure 2. Top panel: residuals of the pulse times-of-arrival (TOAs) for the 2014 ObsIDs 80002092004-09 using the models in Table 5. In the first panel, black dots are the residuals from Model 1 if we ignore the orbital motion, and blue dots include the orbital motion. Green dots add the $\dot{\nu}$ component (Model 2) instead. Bottom panel: residuals of the pulsar TOAs using a timing model similar to Model 3, with two spin derivatives (F0, F1, F2), but changing the orbital period to accommodate one more (purple) or one less (orange) full orbit between ObsIDs 80002092011 and 90201037002. A very obvious modulation at the orbital period, with increasing amplitude, appears in the residuals.

be highly significant (Fig. 1). We only find a hint of pulsation in ObsID 30101045002, close to the predicted

spin-down line and to the detection limit, that we plot in Fig. 4 with a grey point.

Surprisingly, despite not finding the pulsation in any more new observations, we did find a new significant detection in ObsID 80002092004, the second observation of the 2014 campaign, where pulsations were not detected by B14. The reason why this happened is probably because the pulsation departs strongly from the smooth timing noise that was measured back then, shortly after the start of ObsID 80002092006.

3.5. A glitch

Assuming the orbital solution given in Table 4, we fit the data with time models including an increasing number of spin derivatives (Table 5). After adding the F2 ($\ddot{\nu}$) term, besides additional long-term trends that might in principle be described by additional spin derivatives, an abrupt spin frequency change becomes apparent between ObsID 80002092004 and the start of 80002092006 (as shown in Fig. 3). The measured frequency change is too sharp to be described by a small number of additional spin derivatives. It amounts to around $1.7 \cdot 10^{-5}$ Hz, corresponding to $\Delta\nu/\nu \approx 2 \cdot 10^{-5}$ (Table 5).

To exclude instrumental effects, we checked the details of the clock correction file during this time range. We compared the results of the standard clock correction pipeline with a new clock correction based on an improved thermal model of the spacecraft oscillator (Bachetti et al. in prep.), finding a very good agreement

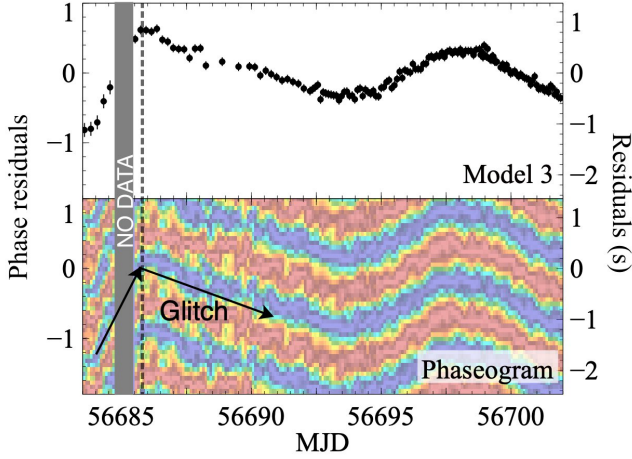


Figure 3. The middle panel and the bottom panels show the residuals and the phaseogram from Model 3, with the glitch at MJD 56685.8 clearly visible (vertical dotted line). The additional “waves” in the residuals are not periodic and can be interpreted as torque red noise.

(well inside the error bars). Bad clock offset measurements from the ground stations could in principle produce changes in the measured pulsed frequency, but we verified that the scatter of the offset measurements from the Malindi station is $\leq 100 \mu\text{sec}$ and we excluded all measurements from other, less reliable, ground stations, with no significant changes in the results.

The measured frequency change of $\Delta\nu/\nu \approx 2 \cdot 10^{-5}$ is a very large value even for a pulsar glitch. Typical glitch magnitudes in radio pulsars are more than an order of magnitude (often many orders of magnitude) smaller; see [Manchester 2018](#) for a review.

We discuss the possible interpretations in the following sections.

4. DISCUSSION

This long observation campaign showed a series of unexpected phenomena, that deserve separate discussion.

4.1. Transient pulsations

M82 X-2 changed dramatically its pulsed fraction in 2014, and in the new observations it often showed no detectable pulsations. Whereas the non-detections after 2014 might be largely due to a high flux of M82 X-1 (see Table 2), the pulsed fraction change in 2014 is not associated with changes of the background flux. Fig. 5 shows that the increase of pulsed fraction is associated with an *increase* of flux and a stable hardness ratio. If a rise in flux from M82 X-1 were the cause for the disappearance of pulsations, we would have expected the pulsed fraction to *decrease* as the total flux increases and vice versa, and maybe a more significant change

Parameter	B14	2014-only fit	All data
T_0 (MJD)	56694.7327(1)	56682.0661(3)	56682.0661(3)
$a \sin i$ (lt-s)	22.225(4)	22.215(5)	22.215(5)
P_{orb} (d)	2.5326(5)*	2.5331(5)	2.53297(2)

Table 4. Updated Orbital parameters of M82 X-2, compared to the B14 fit and to a new fit of the 2014-only data. The fit of the 2014-only data is dependent on how one models the pulse red noise. The quoted uncertainties represent approximate symmetrical $1\text{-}\sigma$ confidence intervals. Values and error bars on $a \sin i$ and T_0 are fixed to the 2014-only value. The 2014-only quoted error bar on the orbital period here uses fits with different red noise models (multiple spin derivatives, WAVE parameters, etc.). The all-data error bar on the orbital period is an estimate based on the uncertainty on T_0 in the 2016 observation (~ 500 s, which gives an error of ~ 1.3 s on the orbital period, propagated over the ~ 950 days between the passages through the ascending node in 2014 and in 2016).

*: The quoted error bar from B14 is unrealistically small; it was most-likely a typo in the original paper, where the correct figure was assigned to the wrong digit.

of hardness ratio as the relative flux of the two sources changes.

This phenomenon of transient pulsations was observed in other accreting pulsars. One notable example is Aql X-1, an accreting millisecond pulsar in a low-mass X-ray binary, a very different system than M82 X-2. [Casella et al. \(2008\)](#) reported pulsations lasting only ~ 150 s over several megaseconds of *RXTE* observations. Another accreting millisecond pulsar, HETE J1900.1-2455, showed transient pulsations during an outburst, with changes of pulsed fraction associated with thermonuclear bursts ([Galloway et al. 2006](#)). Accreting millisecond pulsars are usually found in low-mass X-ray binaries and have low magnetic fields ([Mukherjee et al. 2015](#)). Going to accreting pulsars arguably more similar to M82 X-2 due to their higher luminosities and higher-mass companion stars⁹, there are a few notable examples. A0538-66 showed pulsations in 1982 ([Skinner et al. 1982](#)) and then never since (see [Kretschmar et al. 2004](#), for a review). Recently, [Brumback et al. \(2018\)](#) and [Pike et al. \(2019\)](#) reported on transient pulsations from the X-ray binaries LMC X-4 and SMC X-1. In the first case, a significant change of pulse properties (r.m.s., spin derivative) was associated with the precursor of a

⁹ We note that magnetospheric accretion in accreting pulsars is a delicate balance between the mass accretion rate and the magnetic field strength ([Ghosh & Lamb 1979a](#); [Romanova & Kulkarni 2009](#)). Therefore, it is likely that clues to understand the transient pulsation phenomenon can come by comparing low-mass and high-mass systems.

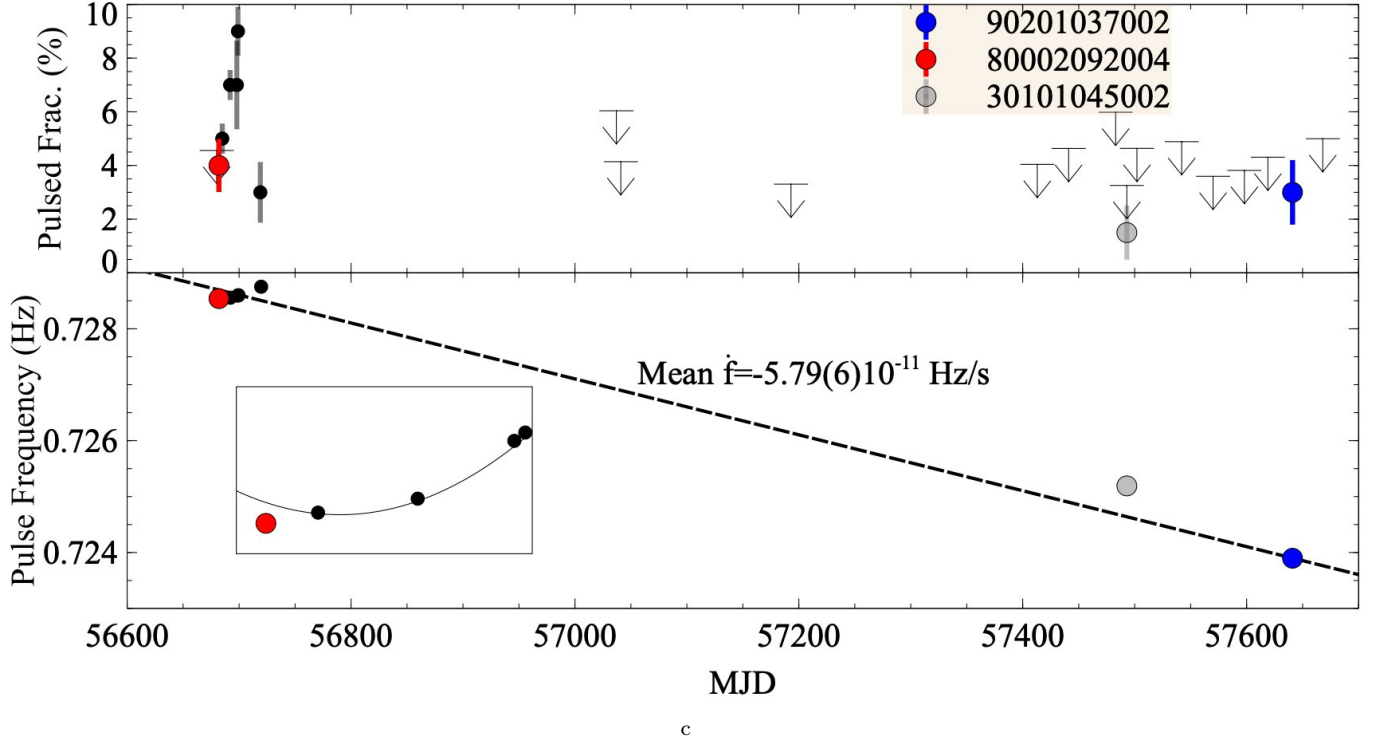


Figure 4. History of detections of pulsations from M82 X-2, showing the mean spin down of the neutron star. The new detections are highlighted with larger markers (including the marginal one in grey). The inset shows the timing solution from Model 3 in Table 5, applied to the data from ObsIDs 80002092004--09. Upper limits are indicated by arrows. Note that for the marginal detection in 30101045002 we plot both the marker and the upper limit.

	Model 1	Model 2	Model 3	Model 4
F0 (Hz)	0.728566160(7)	0.72852171(3)	0.72855082(8)	0.72854408(11)
F1 (10^{-11} Hz/s)	0	4.758(3)	-2.98(2)	-5.29(3)
F2 (10^{-17} Hz/s ²)	0	0	8.66(2)	10.93(3)
GL_F0 (Hz)	0	0	0	$1.75(2) \cdot 10^{-5}$
GLEP (MJD)	—	—	—	56685.8 (fixed)
r.m.s. (μ s)	136	34	9.2	4.3
χ^2 (μ s ²)	2698012	165709	12251	2704

Table 5. Spin parameters for the observations in 2014 using different models. Orbital parameters were fixed to the values in Table 4. The reference epoch for all models is MJD 56683. Note that, even if the F1 term is negative suggesting spin down, the effect of the second spin derivative F2 is dominant and gives spin *up*.

large burst-like flux increase, which is compatible with an increase of the accretion rate at the surface (e.g., the disk overcoming the centrifugal barrier of the magnetized neutron star). In the second there was, instead, evidence of a change of absorption between the non-pulsed and the pulsed intervals, suggesting the presence of occulting material.

A precessing structure that occults the central X-ray source could be the explanation for the periodic modulation of the flux from M82 X-2 (Brightman et al. 2019). A strong disk wind, as observed in several ULXs (e.g. Pinto et al. 2016; Fabrika et al. 2015; Kosec et al. 2018),

would follow a precessing disk and block the view of the central flux from the compact object. For example, Dauser et al. (2017) model long super-orbital periods observed in ULXs as the precession from a disk launching a conical wind. Precession is observed in an archetipal super-critical source, SS433, and various ULXs (Begelman et al. 2006). It is expected to produce a periodic hardening of ULX spectra (Middleton et al. 2015).

Using the best *Chandra* data available, Brightman et al. in prep. do not find a significant spectral evolution of M82 X-2, and in particular no evidence of large variations of N_H , and the spectrum often consistent with the

pulsed spectrum reported by [Brightman et al. \(2016\)](#). However, the N_H is quite high and the spectrum of M82 X-2 hard, with the Galactic X-ray emission dominating the low energies. It is possible that changes of N_H go unnoticed or confused with other degenerate parameters. Also, a highly ionized wind would reduce the flux by scattering rather than the photoelectric effect, reducing the measured N_H .

An additional explanation might involve the precession of the pulsar, with the pulse beam moving away from the observer. In principle, this might be detected through changes of the pulsar spectrum. Given the relatively low count rate of the source, and the large source confusion (with M82 X-1 at 5''), this is not testable on *NuSTAR* data and difficult even from existing *Chandra* spectral data, that are sparse and often affected by pile-up, which affects the higher energies where the pulsed component is more significant. In principle, the large spin down discussed in the next Section might indicate a change of the accretion rate, that could indeed alternate between accretion and no accretion, with the total emission dominated by a disk close to spin equilibrium. With the available data, it is not possible to get a definitive answer.

4.2. Spin behavior: close to equilibrium?

The absence of pulsations for a high fraction of time in this system can be interpreted as long periods where accretion does not make it to the surface *in a stable way*. Indeed, the secular spin-down observed between 2014 and 2016 does suggest that the source might be close to spin equilibrium, with large variations of spin-up or spin-down depending on relatively small changes of the magnetospheric radius R_M around the corotation radius R_{co} . This movement of the disk would also produce a change of the *kind* of accretion, from ordered to unordered when the propeller regime onsets ([Romanova & Kulkarni 2009](#)).

Using the formulae by [Ghosh & Lamb \(1979b\)](#), and assuming constant \dot{M} , one can show that the spin-up of a pulsar should follow a relation

$$-\frac{\dot{p}}{p} \propto p n(\omega_{\text{fast}}) \quad (1)$$

where n is the torque from disk on the magnetic field lines and $\omega_{\text{fast}} = (R_M/R_{co})^{3/2}$ the *fastness parameter*. [Wang \(1995\)](#) derives the following expression for the torque:

$$n(\omega_{\text{fast}}) \approx (7/6 - (4/3)\omega_{\text{fast}} + (1/9)\omega_{\text{fast}}^2)/(1 - \omega_{\text{fast}}) \quad (2)$$

If the pulsar is a *slow* rotator, very far from spin equilibrium, this relation reduces to a constant, $n(\omega_{\text{fast}}) \approx$

7/6, and (1) gives

$$-\frac{\dot{p}}{p} \propto p \quad (3)$$

This relation holds, for example, in NGC 300 ULX-1, that is indeed very far from spin equilibrium ([Vasilopoulos et al. 2018](#)).

However, the spin up shown by M82 X-2 during the 2014 campaign does not follow at all this relation (Fig. 5). Even if we consider a change of \dot{M} proportional to the change of luminosity of the source, we expect a relation of the kind (see [Ghosh & Lamb 1979b](#))

$$-\frac{\dot{p}}{p^2} = \dot{\nu} \propto L_{37}^{6/7} n(\omega_{\text{fast}}) \quad (4)$$

Again, Fig. 5 shows clearly that the spin behavior of M82 X-2 in 2014 is inconsistent with a constant torque, confirming that the source is close to spin equilibrium.

The source might be undergoing some sort of spin reversal over time. This would be similar to what reported for LMC X-4 by [Molkov et al. \(2017\)](#), where an alternating spin up and down behavior was observed over many decades. In that case, one of the possible explanations was a *Recycling magnetosphere model* ([Perna et al. 2006](#)) where accretion is only possible at certain spin phases.

Independently from accretion torque, the pulsar might be spinning down because of its own dipole radiation. According to the classic magnetic dipole radiation formula¹⁰, if the spin down of the pulsar is given by dipole radiation, we can estimate the magnetic field as:

$$B > \left(\frac{3c^3 I}{8\pi^2 R^6} P \dot{P} \right)^{1/2} \approx 3.2 \cdot 10^{19} \left(\frac{P \dot{P}}{s} \right)^{1/2} G \quad (5)$$

where I is the moment of inertia of the neutron star, R its radius, P the pulse period and \dot{P} its period derivative. Let us assume a fine tuned equilibrium from the accretion torque, with no net spin up or down from accretion and the spin down dominated by dipole emission. Substituting the spin period and the spin-down period derivative in the formula above, and using standard estimates for the radius and moment of inertia of the neutron star, we get a lower limit on the magnetic field of $\sim 3 \cdot 10^{14}$ G (Fig. 6). This would be in line with the estimate made by [Tsygankov et al. \(2015\)](#) interpreting the high- and low-luminosity states as the onset of the propeller regime in the source. However, the finding by [Brightman et al. \(2019\)](#) that this flux is periodic would imply that the mass accretion rate changes periodically, switching to the propeller regime every ~ 60 days. Assuming Roche Lobe overflow, possible mechanisms to

¹⁰ See any textbook on pulsars, e.g. <https://www.cv.nrao.edu/course/ast534/Pulsars.html>

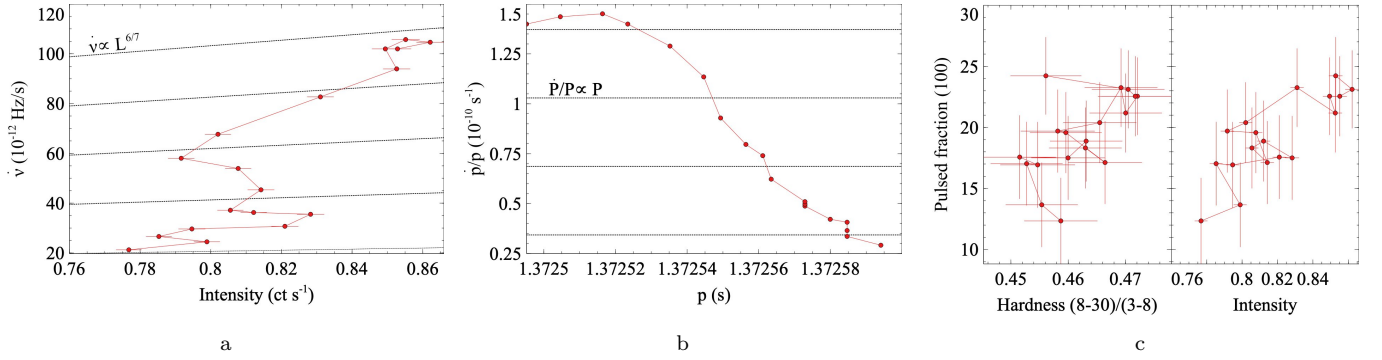


Figure 5. Each point represents 80 ks of data during the 2014 campaign. We calculate spin derivatives from a Savitzky-Golay interpolation of order 2 (Savitzky & Golay 1964, as implemented in `scipy.signal`) of single spin frequency measurements during the campaign. (a) Far from spin equilibrium, we would expect the frequency derivative to be proportional to $L_{37}^{6/7}$ (Ghosh & Lamb 1979b). (b) Some papers cite the relation $\dot{p}/p \propto p$ instead (c) The pulsed fraction increases with total flux. This rules out that a raise of the flux of M82 X-1 is responsible for the disappearance of pulsations.

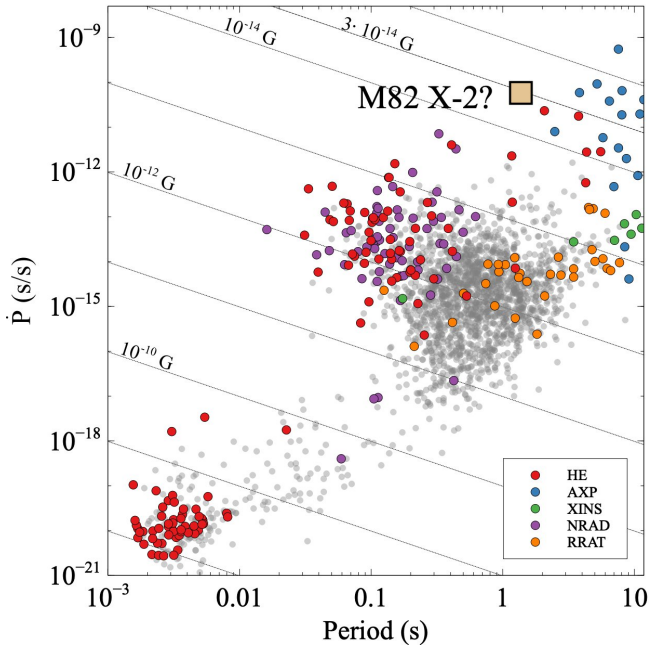


Figure 6. Position of M82 X-2 in the $P-\dot{P}$ diagram under the hypothesis that the measured spin down is mostly rotation-powered. If this were the case, M82 X-2 would have a magnetar-level magnetic field. To produce this figure we used data from the ATNF pulsar catalogue (Manchester et al. 2005)

increase periodically the pressure at the L1 Lagrangian point might involve additional orbiting objects, like the so-called Kozai mechanism (Lidov 1962; Kozai 1962) or tidally excited oscillations (e.g. Fuller 2017). Note that a very small periodic change of orbital eccentricity, well below the quoted upper limit from B14, would be sufficient to produce substantial changes of accretion rate (e.g. Hut & Paczynski 1984; Maccarone et al. 2010). In the same way, a star pulsation could produce a periodic

increase of the mass accretion rate. However, we can exclude an evolved star due to the the small semimajor axis of the orbit Fragos et al. (2015); Heida et al. (2019) and the likely range of companion masses derived from timing (5–20 M_{\odot} , B14). We expect the companion to be a main sequence O-type star, and pulsations reported for these systems (e.g. from β -Cepheids or slowly-pulsating Be stars) are on shorter timescales. (see Samus’ et al. 2017). Stars that can in principle have stable pulsations in the 60-d range are usually evolved either lower-mass stars or luminous blue variables (LBVs), that are thought to be much more massive than the likely 5–20 M_{\odot} range for M82 X-2 (see, e.g. Conroy et al. 2018; Jiang et al. 2018). Note also that Heida et al. (2019) rule out LBVs in the error circle of M82 X-2.

4.3. Glitch: fast spin down before 2014?

Up to now, there is only one reported positive glitch in an accreting system. KS 1947+300 showed a large glitch of $\Delta\nu/\nu \approx 3.5 \cdot 10^{-5}$ in *RXTE* observations in the early 2000s (Galloway et al. 2004), comparable with $\Delta\nu/\nu \approx 2 \cdot 10^{-5}$ reported in Section 3.5. Besides KS 1947+300, glitches of this magnitude have only been reported in magnetars (e.g. Dib et al. 2009; Dib & Kaspi 2014; Archibald et al. 2016), together with *anti*-glitches, sudden slow-downs of the pulsar. A non-magnetar glitch is usually believed to be an adjustment of the NS crust after a change of spin frequency. In radio pulsars, for example, they generally happen after a deceleration of star’s rotation (spin down). Due to its spin, the star is oblated at its equator, and when it slows down due to its dipole radiation, the centrifugal push on its equator decreases. A glitch happens when its solid crust suddenly moves to a more spherical shape. During this event, the moment of inertia of the star decreases and the spin frequency suddenly goes up. The opposite is believed to have happened with the anti-glitch observed

in NGC 300 ULX-1 (Ray et al. 2018). In that case, the authors believe that the strong spin up due to accretion has produced a centrifugal pull on the crust that has led to a larger oblateness of the surface. In our case, given the observed secular spin down, it is possible that the glitch we observe at epoch 56685.8 is a standard glitch, due to a possible accretion-torque spin down, instead of a rotation-powered spin down, prior to the 2014 observations. Another option would be that the process involved here is due to a high magnetic field, like in magnetars. This would agree with the secular spin down being due to dipole radiation.

We do not have enough data to test this hypothesis.

4.4. *Would a high magnetic field imply an electron capture origin?*

The findings of Sections 3.3.0.0 and 3.5 can be interpreted as signatures of a very high magnetic field. The idea of a magnetar-scale magnetic field in a binary, however, is puzzling. A typical supernova explosion will result in the loss of a substantial fraction of the mass from the supernova progenitor, which will usually be the heavier object in a binary. When more than half the total mass in the system is lost, the binary becomes entirely unbound. With more modest mass loss, the binary becomes eccentric and acquires a longer orbital period than it had before the merger (e.g. Boersma 1961). In such systems, accretion can take place only for a small range of orbital phases very close to periastron, which would suppress accretion. Given that the typical decay timescale for a magnetar’s magnetic field is of order 10000 years, but that the circularization timescale for donor stars with radiative envelopes is much longer than this, the combination of a nearly circular orbit with a magnetar-like magnetic field requires some explanation.

In principle, a very finely tuned asymmetry of the supernova explosion can “fix” some of the problems caused by mass loss, but these systems will have long orbital periods (Kalogera 1998). The alternative solution is to require a minimal mass loss. This can be done by electron capture supernova processes, which which an iron core never forms, and can result either from the collapse of intermediate mass stars (e.g. Nomoto 1987; Poelarends et al. 2008) or accretion induced collapse of a white dwarf in a binary (Ergma 1993; Fryer et al. 1999). Some observations of accreting X-ray pulsars suggest that there are two sets of these objects, with reasonable albeit not airtight arguments that some form in core collapse supernovae and others form in electron capture supernovae (Pfahl et al. 2002; Knigge et al. 2011). These systems are expected to have not just lower sym-

metric kicks due to mass loss (Blaauw 1961), but also lower asymmetric kicks (Fryer et al. 1999).

A few other aspects of this scenario are additionally attractive. First, evolutionary calculations show a preference for donors of about 5-10 M_{\odot} (Fragos & McClintock 2015). The masses of stars in binaries tend to show correlations, with a flat mass ratio distribution, rather than the mass ratio distribution predicted by randomly drawing from a standard initial mass function law (Sana et al. 2012). The direct electron capture supernovae tend to occur for progenitor masses of about 8-10 M_{\odot} (Nomoto 1987), while the white dwarfs with small enough carbon abundances that they can undergo accretion induced collapses have progenitor masses just below the range required for supernovae to occur (Canal & Schatzman 1976). Furthermore, there are widespread suggestions that accretion-induced collapse and/or merger-induced collapse events (i.e. those in which the merger of two white dwarfs drives a collapse to a neutron star) can lead to the production of magnetars (e.g. Usov 1992; King et al. 2001). Additionally, the lack of a supernova remnant associated with such a young system also favors the idea that the neutron star formed in a manner with much less mass ejection than typical core collapse supernovae. If indeed the magnetic field is high as suggested by the spin down and the glitch (and as previously suggested for this source in the literature, e.g. Tsygankov et al. 2015, Mushtukov et al. 2015, Ekşi et al. 2015, Dall’Osso et al. 2015), there is, thus, an intriguing range of indirect evidence that this system has formed via accretion-induced collapse of a white dwarf, but the evidence at the present time is far from conclusive.

4.5. *An orbital period derivative?*

As reported in Section 3.3 and Table 4, if we select only the data from the 2014 observations and fit the orbital parameters, we obtain a slightly different orbital period than measured including the 2016 dataset. This might in principle mean that the orbit has shrunk and the orbital period has decreased over time, due for example to the strong mass exchange that the super-Eddington luminosity of the source seems to imply. However, the 2014 observations contain a strong timing noise, that might have influenced the fit of the orbit reported by B14 and adjusted in this Paper. We find slightly different solutions depending on the model for the red noise, and Table 4 sums up this variability through larger error bars than calculated from the single fits.

However, if the reported tension between the 2014-only orbital solution and the one with the full data set

is true, a single new measurement of the orbital phase in future observations (at this point more than three years since the last one) will be able to measure with high significance a negative orbital period derivative. The values in Table 4 would imply $\dot{P}_{\text{orb}} \sim -10^{-7}$ d/d implying an orbital evolution time-scale of 30000 yrs and a mass exchange almost three orders of magnitude above the Eddington limit (see below).

Following Rappaport et al. (1982), the expected orbital period derivative for mass transfer from a more massive companion star, neglecting a contribution from gravitational waves, can be estimated through

$$\frac{\dot{a}}{a} = \frac{2\dot{P}_{\text{orb}}}{3P_{\text{orb}}} = -\frac{\dot{M}_c}{M_c} \left[2 \left(1 - \frac{\beta}{q} \right) - \frac{1-\beta}{1+q} - \frac{2\alpha(1-\beta)(1+q)}{q} \right] \quad (6)$$

where M_c and \dot{M}_c are the mass and mass loss from the companion (negative), M_p and \dot{M}_p the same quantities for the pulsar, $q = M_p/M_c$, $\beta = -\dot{M}_p/\dot{M}_c$, and α the specific angular momentum of the lost mass in units of $2\pi a_p^2/P_{\text{orb}}$. In the conservative scenario, $\beta = 1$ and (6) becomes

$$\frac{\dot{a}}{a} = \frac{2\dot{P}_{\text{orb}}}{3P_{\text{orb}}} = -\frac{\dot{M}_c}{M_c} \left[2 \left(1 - \frac{1}{q} \right) \right] \quad (7)$$

In the scenario where all mass is lost in an outflow before accreting on the pulsar, but the outflow is launched from close to the pulsar, the specific angular momentum is $j_{\text{outflow}} \approx 2\pi a_p^2/P_{\text{orb}}$, where a_p is the semimajor axis of the pulsar orbit. Therefore $\beta = 0$ and

$$\alpha \approx \left(\frac{a_p}{a} \right)^2 = \left(\frac{M_c}{M_p + M_c} \right)^2 = \frac{1}{(1+q)^2}$$

and the (6) reduces to

$$\frac{\dot{a}}{a} = \frac{2\dot{P}_{\text{orb}}}{3P_{\text{orb}}} = -\frac{\dot{M}_c}{M_c} \left[2 - \frac{2+q}{q(1+q)} \right] \quad (8)$$

which is a relatively small correction to (7) for small values of q .

If the mass transfer in the system is highly super Eddington and no significant mass losses happen close to the donor star, both scenarios predict that the orbit shrinks, with orbital period derivatives of the order

$$\dot{P}_{\text{orb}} \sim -0.015 \left(\frac{M_p}{1.4M_{\odot}} \right)^{-1} \left(\frac{-\dot{M}_c}{M_{\odot}/\text{yr}} \right) \quad (9)$$

$$\sim -3.5 \cdot 10^{-8} \left(\frac{M_p}{1.4M_{\odot}} \right)^{-1} \left(\frac{-\dot{M}_c}{100\dot{M}_{\text{Edd}}} \right) \quad (10)$$

This \dot{P}_{orb} corresponds to a change of orbital period of ~ 1 s/yr, and produces a shift of the orbital phase by a

few 100 s over a few years. Again, since \dot{M}_c is negative, also this \dot{P}_{orb} is negative. This is easy to observe with standard techniques of pulsar timing. Future observations will test this hypothesis by tracking the orbital phase over time.

Finally, the remaining extreme scenario where most mass is lost from the system in form of winds from the donor star, we have

$$\frac{\dot{a}}{a} = \frac{2\dot{P}_{\text{orb}}}{3P_{\text{orb}}} = -\frac{\dot{M}_c}{M_c} \frac{1}{(1+q)} \quad (11)$$

It is easy to show that this scenario would bring the orbit to *expand* instead of shrinking (positive \dot{P}_{orb}).

It is likely that in a real-life scenario both phenomena should happen, stabilizing the mass transfer over long time scales. Fragos et al. (2015) discuss these arguments in detail. The detection of an orbital period derivative would set strong constraints on the viable models for the evolution of the binary system in M82 X-2.

5. CONCLUSIONS

This work characterizes the timing behavior of M82 X-2 over two years, showing a number of phenomena that can be used to understand the nature of this remarkable source. None of these new findings provide definitive information on the nature of the source, but they represent important clues. Thanks to this work, we now know that:

- The pulsar alternates phases with a large spin up to phases with a large spin down. Moreover, the spin-up is inconsistent with small values of the fastness parameter. This is a strong indication that the pulsar is close to spin equilibrium.
- The pulsations are transient, changing their significance over time, with a tentative positive correlation with the flux of the source. This points to an intrinsic mechanism for this pulsed fraction variability rather than, e.g., a change of the background flux from the nearby M82 X-1.
- The neutron star has very strong glitches, probably due to the rapid spin evolution. The observed glitch probably implies a strong spin down prior to the first detection in 2014.

In addition, we now have a very precise orbital solution, that can be used to look for orbital phase derivatives in future observations. This will be crucial to test the total mass exchange in the system.

MB thanks the Fulbright Visiting Scholar Program for supporting a nine-month visit at Caltech. The authors

wish to thank Jim Fuller for insightful conversations on stellar pulsations.

Facilities: *NuSTAR* (Harrison et al. 2013), *Chandra* (Weisskopf et al. 2002), ATNF pulsar catalogue (Manchester et al. 2005)

Software: Stingray (Huppenkothen et al. 2016; Huppenkothen et al. 2019), HENDRICS (Bachetti 2018), astropy (Price-Whelan et al. 2018), PINT (Luo et al. 2019), PRESTO (Ransom 2011)

REFERENCES

- Andersen, B. C., & Ransom, S. M. 2018, *The Astrophysical Journal*, **863**, L13
- Archibald, R. F., Kaspi, V. M., Tendulkar, S. P., & Scholz, P. 2016, *The Astrophysical Journal*, **829**, L21
- Bachetti, M. 2018, *Astrophysics Source Code Library*, ascl:1805.019
- Bachetti, M., Harrison, F. A., Walton, D. J., et al. 2014, *Nat.*, **514**, 202
- Begelman, M. C., King, A. R., & Pringle, J. E. 2006, *Monthly Notices of the Royal Astronomical Society*, **370**, 399
- Blaauw, A. 1961, *\bain*, **15**, 265
- Boersma, J. 1961, *\bain*, **15**, 291
- Brightman, M., Harrison, F., Walton, D. J., et al. 2016, *ApJ*, **816**, 60
- Brightman, M., Harrison, F. A., Bachetti, M., et al. 2019, *The Astrophysical Journal*, **873**, 115
- Brumback, M. C., Hickox, R. C., Bachetti, M., et al. 2018, *The Astrophysical Journal*, **861**, L7
- Buccheri, R., Bennett, K., Bignami, G. F., et al. 1983, *A&A*, **128**, 245
- Canal, R., & Schatzman, E. 1976, *Astronomy and Astrophysics*, **46**, 229
- Carpano, S., Haberl, F., Maitra, C., & Vasilopoulos, G. 2018, *MNRAS Let.*, **476**, L45
- Casella, P., Altamirano, D., Patruno, A., Wijnands, R. A. D., & van der Klis, M. 2008, *ApJ*, **674**, L41
- Conroy, C., Strader, J., van Dokkum, P., et al. 2018, *The Astrophysical Journal*, **864**, 111
- Dall’Osso, S., Perna, R., & Stella, L. 2015, *MNRAS*, **449**, 2144
- Dauser, T., Middleton, M., & Wilms, J. 2017, *Monthly Notices of the Royal Astronomical Society*, **466**, 2236
- Dib, R., & Kaspi, V. M. 2014, *ApJ*, **784**, 37
- Dib, R., Kaspi, V. M., & Gavriil, F. P. 2009, *The Astrophysical Journal*, **702**, 614
- Ekşi, K. Y., Andaç, İ. C., Çikintoğlu, S., et al. 2015, *MNRAS Let.*, **448**, L40
- Ergma, E. 1993, *\aap*, **273**, L38
- Fabrika, S., Ueda, Y., Vinokurov, A., Sholukhova, O., & Shidatsu, M. 2015, *Nature Physics*, **11**, 551
- Fragos, T., Linden, T., Kalogera, V., & Skias, P. 2015, *The Astrophysical Journal*, **802**, L5
- Fragos, T., & McClintock, J. E. 2015, *The Astrophysical Journal*, **800**, 17
- Fryer, C., Benz, W., Herant, M., & Colgate, S. A. 1999, *\apj*, **516**, 892
- Fuller, J. 2017, *Monthly Notices of the Royal Astronomical Society*, **472**, 1538
- Fürst, F., Walton, D. J., Harrison, F. A., et al. 2016, *ApJL*, **831**, L14
- Galloway, D. K., Morgan, E. H., Krauss, M. I., Kaaret, P., & Chakrabarty, D. 2006, *ApJ*, **654**, L73
- Galloway, D. K., Morgan, E. H., & Levine, A. M. 2004, *The Astrophysical Journal*, **613**, 1164
- Ghosh, P., & Lamb, F. K. 1979a, *ApJ*, **232**, 259
- . 1979b, *ApJ*, **234**, 296
- Harrison, F. A., Craig, W. W., Christensen, F. E., et al. 2013, *ApJ*, **770**, 103
- Heida, M., Harrison, F. A., Brightman, M., et al. 2019, *The Astrophysical Journal*, **871**, 231
- Huppenkothen, D., Bachetti, M., Stevens, A. L., Migliari, S., & Balm, P. 2016, *Astrophysics Source Code Library*, ascl:1608.001
- Huppenkothen, D., Bachetti, M., Stevens, A. L., et al. 2019, arXiv e-prints, arXiv:1901.07681
- Hut, P., & Paczynski, B. 1984, *The Astrophysical Journal*, **284**, 675
- Israel, G. L., Belfiore, A., Stella, L., et al. 2017a, *Science*, **355**, 817
- Israel, G. L., Papitto, A., Esposito, P., et al. 2017b, *MNRAS Let.*, **466**, L48
- Jiang, Y.-F., Cantiello, M., Bildsten, L., et al. 2018, arXiv e-prints, arXiv:1809.10187
- Kalogera, V. 1998, *\apj*, **493**, 368
- King, A. R., Pringle, J. E., & Wickramasinghe, D. T. 2001, *\mnras*, **320**, L45
- Knigge, C., Coe, M. J., & Podsiadlowski, P. 2011, *\nat*, **479**, 372
- Koliopanos, F., Vasilopoulos, G., Godet, O., et al. 2017, *A&A*, **608**, A47

- Kosec, P., Pinto, C., Walton, D. J., et al. 2018, [Monthly Notices of the Royal Astronomical Society](#), 479, 3978
- Kozai, Y. 1962, [The Astronomical Journal](#), 67, 591
- Kretschmar, P., Wilms, J., Stauber, R., Kreykenbohm, I., & Heindl, W. A. 2004, in [Proceedings of the 5th INTEGRAL Workshop on the INTEGRAL Universe \(ESA SP-552\)](#). 16-20 February 2004, 329
- Lidov, M. L. 1962, [Planetary and Space Science](#), 9, 719
- Luo, J., Ransom, S., Demorest, P., et al. 2019, [Astrophysics Source Code Library](#), ascl:1902.007
- Maccarone, T. J., Kundu, A., Zepf, S. E., & Rhode, K. L. 2010, [Monthly Notices of the Royal Astronomical Society](#), 409, L84
- Manchester, R. N. 2018, [arXiv:1801.04332 \[astro-ph\]](#), 1801.04332
- Manchester, R. N., Hobbs, G. B., Teoh, A., & Hobbs, M. 2005, [The Astronomical Journal](#), 129, 1993
- Middleton, M. J., Heil, L., Pintore, F., Walton, D. J., & Roberts, T. P. 2015, [MNRAS](#), 447, 3243
- Middleton, M. J., & King, A. 2017, [Monthly Notices of the Royal Astronomical Society](#), 470, L69
- Molkov, S., Lutovinov, A., Falanga, M., Tsygankov, S., & Bozzo, E. 2017, [Monthly Notices of the Royal Astronomical Society](#), 464, 2039
- Mukherjee, D., Bult, P., van der Klis, M., & Bhattacharya, D. 2015, [Monthly Notices of the Royal Astronomical Society](#), 452, 3994
- Mushtukov, A. A., Suleimanov, V. F., Tsygankov, S. S., & Poutanen, J. 2015, [arXiv](#), 3600
- Nomoto, K. 1987, [apj](#), 322, 206
- Perna, R., Bozzo, E., & Stella, L. 2006, [The Astrophysical Journal](#), 639, 363
- Pfahl, E., Rappaport, S., Podsiadlowski, P., & Spruit, H. 2002, [apj](#), 574, 364
- Pike, S. N., Harrison, F. A., Bachetti, M., et al. 2019, [arXiv e-prints](#), [arXiv:1903.06306](#)
- Pinto, C., Fabian, A., Middleton, M., & Walton, D. 2016, [arXiv](#), [arXiv:1611.00623](#), [arXiv: 1611.00623](#)
- Pintore, F., Zampieri, L., Stella, L., et al. 2017, [The Astrophysical Journal](#), 836, 113
- Poelarends, A. J. T., Herwig, F., Langer, N., & Heger, A. 2008, [apj](#), 675, 614
- Price-Whelan, A. M., , Gnther, H. M., et al. 2018, [arXiv](#), [arXiv:1801.02634](#), [arXiv: 1801.02634](#)
- Ransom, S. 2011, [Astrophysics Source Code Library](#), ascl:1107.017
- Ransom, S. M. 2001, PhD thesis, Harvard University
- Ransom, S. M., Eikenberry, S. S., & Middleditch, J. 2002, [The Astronomical Journal](#), 124, 1788
- Rappaport, S., Joss, P. C., & Webbink, R. F. 1982, [ApJ](#), 254, 616
- Ray, P. S., Guillot, S., Ho, W. C. G., et al. 2018, [arXiv e-prints](#), [arXiv:1811.09218](#)
- Romanova, M. M., & Kulkarni, A. K. 2009, [MNRAS](#), 398, 1105
- Samus', N. N., Kazarovets, E. V., Durlevich, O. V., Kireeva, N. N., & Pastukhova, E. N. 2017, [Astronomy Reports](#), 61, 80
- Sana, H., de Mink, S. E., de Koter, A., et al. 2012, [Science](#), 337, 444
- Savitzky, A., & Golay, M. J. E. 1964, [Anal. Chem.](#), 36, 1627
- Skinner, G. K., Bedford, D. K., Elsner, R. F., et al. 1982, [Nature](#), 297, 568
- Taylor, J. H., & Weisberg, J. M. 1982, [ApJ](#), 253, 908
- Tsygankov, S. S., Mushtukov, A. A., Suleimanov, V. F., & Poutanen, J. 2015, [arXiv](#), 8288
- Usov, V. V. 1992, [nat](#), 357, 472
- Vasilopoulos, G., Haberl, F., Carpano, S., & Maitra, C. 2018, [Astronomy and Astrophysics](#), 620, L12
- Walton, D. J., Fürst, F., Heida, M., et al. 2018, [The Astrophysical Journal](#), 856, 128
- Wang, Y.-M. 1995, [ApJL](#), 449, L153
- Weisskopf, M. C., Brinkman, B., Canizares, C., et al. 2002, [The Publications of the Astronomical Society of the Pacific](#), 114, 1
- Wiktorowicz, G., Lasota, J.-P., Middleton, M., & Belczynski, K. 2018, [arXiv e-prints](#), [arXiv:1811.08998](#)

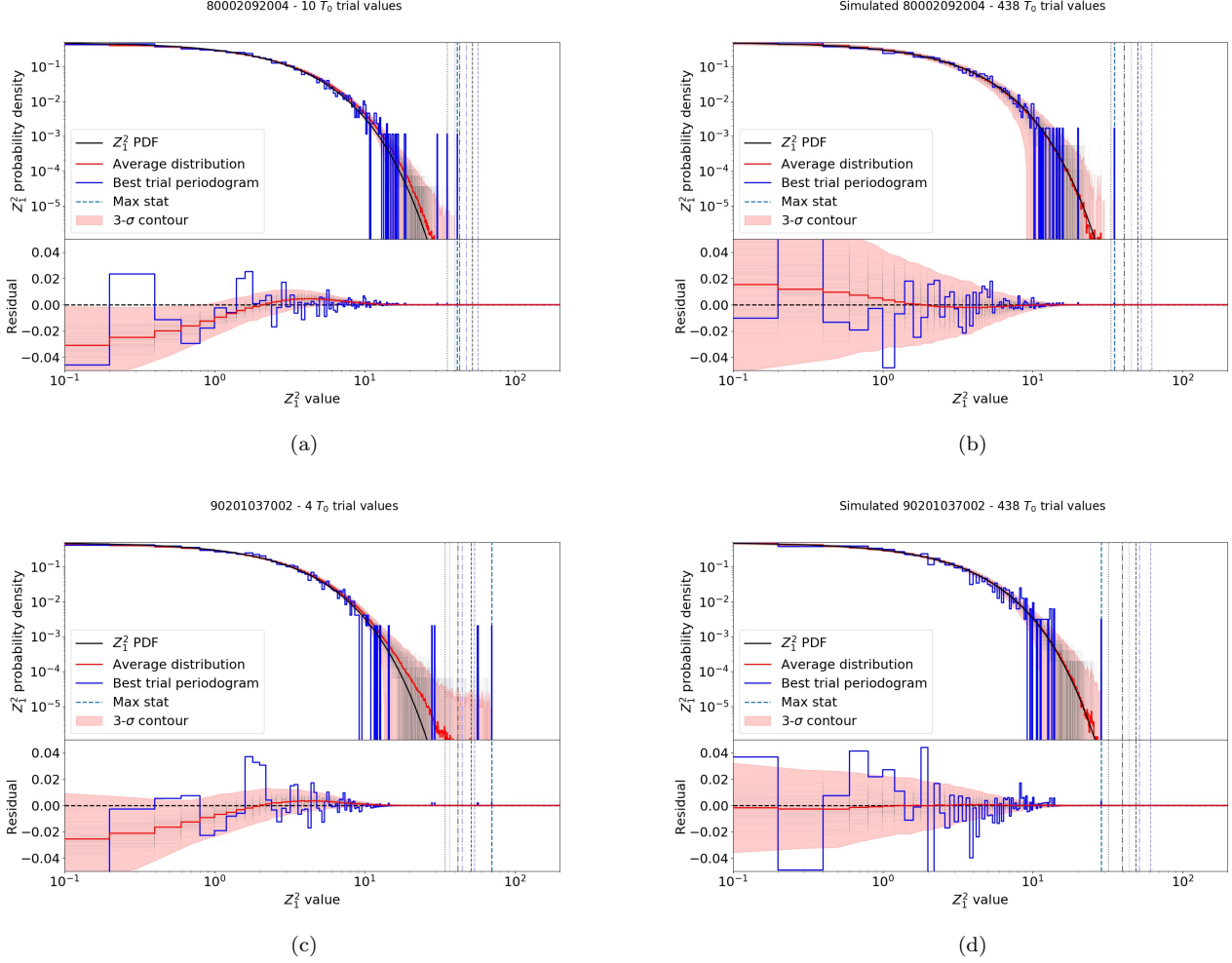


Figure 7. The statistical distribution of Z_1^2 values in our blind search of pulsations, using the orbital solution in Table 4 and a search over T_0 values and f, \dot{f} . The dotted, dash-dotted and dashed vertical lines show the 3, 4 and 5- σ levels from the theoretical distribution, for the case of a single search over $f - \dot{f}$, and accounting for the given number of trial values of T_0 . a/b show ObsID 80002092004 in 2014. The detection significance is barely above 3- σ if considered as a blind search, but the spin values and the inferred T_0 are very close to the values in ObsID 80002092006, which increases the reliability of this detection. c/d show the same plot for the new detection in ObsID 90201037002, showing a detection significance well above 5- σ .

APPENDIX

A. ON THE DETECTION LIMITS USED IN THE PULSATION SEARCH.

Fig. 7 shows the statistical distribution of Z_n^2 values during a search for pulsations with the methods described in Section 3.4. We executed the analysis on real data, and on (hundreds of realizations of) simulated data with the same GTIs and count rate as the original observation. In a search containing only simulated white noise, the statistical distribution follows very closely the expected χ^2 distribution (Buccheri et al. 1983). This means that the folding-and-shift procedure, with a careful choice of parameters, does not alter significantly the null-hypothesis probability, that can be used to search for pulsations.

We conclude that the slight deviations from the white-noise statistical distribution found in real data are driven by the source variability and not from the analysis technique used.

To evaluate the p -value, in order not to increase synthetically the number of trials, we consider only the trials over T_0 needed to get the best detection: if the best T_0 is very close to the known orbit, it means that the search over the full T_0 space is noise without any added value.